

# Rich Action-semantic Consistent Knowledge for Early Action Prediction

Xiaoli Liu, *Student Member, IEEE*, Jianqin Yin, *Member, IEEE* and Di Guo, *Member, IEEE*,

**Abstract**—Early action prediction (EAP) aims to recognize human actions from a part of action execution in ongoing videos, which is an important task for many practical applications. Most prior works treat partial or full videos as a whole, ignoring rich action knowledge hidden in videos, i.e., semantic consistencies among different partial videos. In contrast, we partition original partial or full videos to form a new series of partial videos and mine the Action Semantic Consistent Knowledge (ASCK) among these new partial videos evolving in arbitrary progress levels. Moreover, a novel Rich Action-semantic Consistent Knowledge network (RACK) under the teacher-student framework is proposed for EAP. Firstly, we use a two-stream pre-trained model to extract features of videos. Secondly, we treat the RGB or flow features of the partial videos as nodes and their action semantic consistencies as edges. Next, we build a bi-directional semantic graph for the teacher network and a single-directional semantic graph for the student network to model rich ASCK among partial videos. The MSE and MMD losses are incorporated as our distillation loss to enrich the ASCK of partial videos from the teacher to the student network. Finally, we obtain the final prediction by summering the logits of different sub-networks and applying a softmax layer. Extensive experiments and ablative studies have been conducted, demonstrating the effectiveness of modeling rich ASCK for EAP. With the proposed RACK, we have achieved state-of-the-art performance on three benchmarks. The code will be released if the paper is accepted.

**Index Terms**—Action prediction, Teacher-student network, Knowledge distillation, Graph neural network.

## 1 INTRODUCTION

Early action prediction (EAP) is an important task in a series of applications ranging from intelligent surveillance, and self-driving to human-robot interaction [1], [2]. Different from traditional action recognition tasks, as shown in Fig. 1, the EAP aims to predict the semantic label of ongoing actions very early before the action is completely executed. Due to the limited observations, the action semantics of partial videos are ambiguous, especially at the very early stages. According to the definitions of EAP, the same action execution with different progress levels of videos shares the same action semantics. Therefore, Partial videos involving different progress levels have various feature distributions and significant intra-class variations. As a result, EAP is particularly challenging, especially predicting action semantics very early.

We assume that the same action semantics have similar feature distributions. Similar distributions of partial videos can be measured by correlations of their features, which is called action-semantic consistent modeling. Through pairwise action-semantic consistent modeling shown in Fig. 2, we can learn similar distributions and their action-semantic consistencies, and we name it Action Semantic Consistent Knowledge (ASCK). Therefore, modeling ASCK among arbitrary partial videos is an intuitive way to learn the similar distributions of their features for alleviating the large intra-

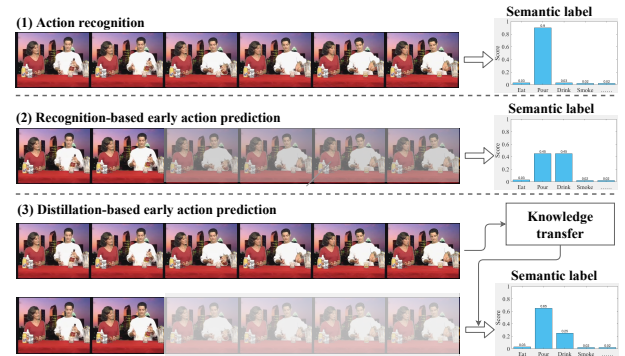


Fig. 1. Action recognition VS early action prediction (EAP). (1) The action recognition model achieves an accurate result of “Pour” from a complete action sequence. (2) The recognition-based EAP model results in ambiguous predictions of “Pour” and “Drink” directly from an incomplete action sequence. (3) The distillation-based EAP model obtains improved results by transferring additional knowledge from the full video.

class variances of partial videos.

Many prior works have been proposed for EAP, mainly including recognition-based methods and distillation-based methods. As shown in Fig. 1, the recognition-based methods directly predict semantic labels of partial videos which contain limited observed sequences with incomplete action executions [3], [4], [5]. For example, Sun et al. [4] proposed a discriminative relational recurrent network (DR2N) and modeled spatiotemporal interactions between actors of several historical frames for predicting future actions. As shown in Fig. 1, due to limited observations, the partial video shares ambiguous semantics of “Pour” and

- Xiaoli Liu and Jianqin Yin are the School of Artificial Intelligence of Beijing University of Posts and Telecommunications, No.10 Xitucheng Road, Haidian District, Beijing 100876, China. Jianqin Yin is the corresponding author. E-mail: Liuxiaoli134@bupt.edu.cn, jqyin@bupt.edu.cn.
- Di Guo is with the Department of Computer Science and Technology of Tsinghua University, Beijing 100084, China.

Manuscript received January 13, 2022; revised January 13, 2022.

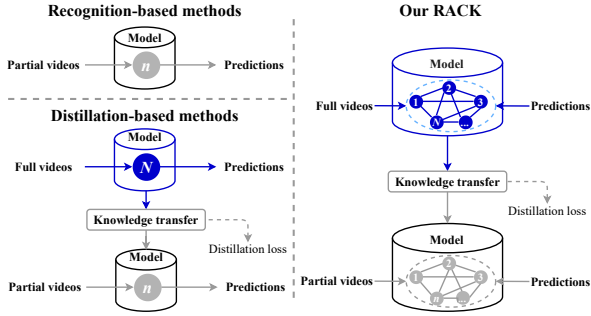


Fig. 2. Different pipelines for early action prediction. The gray dots denote the information from full videos, the blue dots denote the information from partial videos, and the numbers in the dots denote the progress levels of related videos. The left one denotes two general pipelines for EAP, and the right one shows the pipeline of our RACK.

“Drink”, which inevitably leads to poor performance by the recognition-based methods.

The distillation-based methods transfer additional action knowledge from full videos for the missing information of partial videos, which can effectively reduce the ambiguous semantics for predictions [6], [7], [8]. However, as shown in Fig. 2, most existing works treat the partial or full videos as a whole, ignoring the action-semantic knowledge among partial videos with lower progress levels hidden in the original video. Therefore, these models suffer from the limited ability to capture richer ASCK for accurate predictions. By contrast, as shown in Fig. 2, we partition original partial or full videos into a series of new partial videos with arbitrary progress levels. We model rich ASCK among these new partial videos for predictions.

In this paper, we propose a novel Rich Action-semantic Consistent Knowledge network (RACK) under the teacher-student framework for EAP. Specifically, we build the teacher network using a bi-directional fully connected graph with partial videos as nodes. The teacher network distills ASCK among partial videos from lower progress levels to higher progress levels and higher progress levels to lower progress levels. The student network is built with a single-directional fully connected graph since future information is not available during the testing phase. The student network distills ASCK among partial videos from lower progress levels to higher progress levels. We further transfer the ASCK from full to partial videos via layer-wise distillation loss between teacher and student networks. With these elegant designs, the student network also distills ASCK from higher progress levels to lower progress levels for predictions. Moreover, we extract two-stream features as the representation of partial or full videos, including RGB and flow features. We obtain the logits of RGB or flow modalities by feeding the two-stream features to RACK, respectively. Finally, we summarize these logits and obtain the predictions via a softmax layer. In contrast to [8], we capture richer ASCK among partial videos with arbitrary progress levels instead of adjacent partial videos. We have achieved a new state-of-the-art performance on three benchmarks (i.e., UCF101, HMDB51, Something Something V2), showing the effectiveness of modeling rich ASCK.

Our main contributions are three folds.

- To the best of our knowledge, we are the first to explore rich ASCK among arbitrary partial videos, which helps to learn similar feature distributions of partial videos with the same action execution for accurate predictions.
- We propose a novel RACK model via the teacher-student framework for EAP. The proposed method models rich action knowledge via graph-based knowledge reasoning and a knowledge distillation framework, which helps reduce large intra-class variances for accurate predictions.
- Experimental results show our new state-of-the-art performance on three datasets, demonstrating the effectiveness of our method. The ablative analysis further shows that modeling rich ASCK can effectively improve predictions.

## 2 RELATED WORK

### 2.1 Early Action prediction

Most of the existing works follow the pipeline of action recognition by directly recognizing the semantic label from partial observations [9], [10], [11]. Kong et al. [12] proposed a men-LSTM model to remember the hard-to-predict samples, which forced their model to learn a more complex classified boundary for accurate predictions. Similarly, Li et al. [13] modeled relationships between similar action pairs and dynamically marked the hard-predicted similar pairs for 3D skeleton-based EAP. Wu et al. [14] and Yao et al. [15] modeled interaction relationships and their evolutions for EAP. Li et al. [16], [17] mined sequential temporal patterns via causality of continuing action units, context cue, and action predictability for the long-duration action prediction. The recognition-based methods easily suffered from poor performance due to the limited observations and large intra-class variations among partial videos with different progress levels.

Many works struggled to reconstruct missing information of partial videos by predicting future information [18], [19], [20] or distilling action knowledge from full videos with complete action executions [7], [8], [21]. For example, some works were proposed to jointly learn future motions and relationships between the observed and future information for early predictions [22], [23], [24]. Kong et al. [21] exploited abundant sequential context features from full videos to enrich and reconstruct the features of partial videos. Cai et al. [7] learned feature embeddings by transferring the knowledge between partial and full videos. Wang et al. [8] learned progressive action knowledge between adjacent partial videos but ignored semantic consistencies of partial videos between lower and higher progress levels, suffering from the limited ability to learn rich action knowledge. By contrast, we model rich ASCK among arbitrary partial videos via densely graph relationship modeling.

### 2.2 Graph neural network (GNN)

Traditional graph neural networks have been deployed for the non-Euclidean data, such as point cloud and human skeleton data [25]. For example, many researchers treated human body joints as nodes and their relationships as edges

for the skeleton-based action recognition [26], [27] or human motion prediction [28]. Recently, GNN has been extended to a series of visual tasks [29], [30], [31]. Liu et al. [32] treated the videos as the 3D point clouds for learning video representations. Zhao et al. [33] and Xu et al. [34] took video snippets as nodes and their relationships as edges to exploit the correlations among video snippets for temporal action detection. Similarly, Zeng et al. [35] built an action proposal graph to exploit the relationships between proposals for temporal action detection. Bai et al. [36] proposed a boundary content GNN (BC-GNN) to model the relationships between temporal proposals' boundary and action content. Wang et al. [30] represented the videos as space-time region graphs by treating the object region proposals as nodes for video-based action recognition. Li et al. [37] transformed a video as a graph with each frame as the node, capturing low-level global temporal clues for recognition.

As discussed above, prior video graphs modeled temporal relationships between video snippets or frames instead of the action semantics of action videos. Due to domain gaps of different tasks, these video graphs can not be directly adopted for EAP. In this paper, we treat the whole partial or full videos as nodes and their semantic consistencies as edges. In this way, we model the action-semantic consistencies between different videos, which is different from the existing works.

### 2.3 Knowledge distillation

Knowledge distillation models were mainly achieved via the teacher-student framework. The teacher-student framework was originally proposed for model compression, which distilled knowledge from a cumbersome teacher network to a lightweight student network [38], [39]. Recently, Cai et al. [7] and Wang et al. [8] introduced the knowledge distillation model for EAP. These models tried to distill action knowledge from full videos by the teacher network and transferred it to the partial videos by the student network. However, Cai et al. [7] ignored semantic correlations among different partial or full videos, and Wang et al. [8] modeled correlations between adjacent partial videos. In contrast to [7] and [8], we consider rich semantic correlations between any partial or full videos and model their ASCK.

## 3 METHODOLOGY

### 3.1 Problem formulation

Consistent with the existing works [1], [8], [21], we assume that a video contains the action with complete executions. Given a video  $X$ , we uniformly partition it into  $N$  segments as  $\{x_1, x_2, \dots, x_N\}$ . The first  $n$  segments form a partial video  $X_n = [x_1, x_2, \dots, x_n]$  with a progress level of  $n$ , and its observation ratio is defined as  $n/N$ , which represents the action completion degree. Early action prediction (EAP) can be formulated as equation 1.

$$c_n = f(X_n, n) \quad (1)$$

where  $f(\cdot)$  is a mapping that transforms a partial video,  $X_n$  into a semantic label  $c_n$ ,  $n$  denotes the progress level of partial video  $X_n$ , and  $n < N$  for the EAP.

As shown in Fig. 2, the distillation-based models utilize full videos to obtain additional information for partial videos with incomplete action execution, effectively assisting predictions. Following this pipeline, we build an RACK network under the teacher-student framework to parameterize  $f(\cdot)$  in section 3.2. In contrast to prior works, we model rich ASCK among partial videos with arbitrary progress levels, which assists in learning missing information and reducing the semantic ambiguities of partial videos.

### 3.2 Early action prediction

Fig. 3 shows our RACK network under the two-stream framework for EAP, which respectively takes RGB and optical flow images as inputs, including RACK-RGB and RACK-Flow. Each stream mainly includes the teacher network, student network, and loss. The teacher or student network learns ASCK of partial videos hidden in the original videos, respectively. The ASCK is transferred from the teacher to the student via the distillation loss, which enriches the ASCK of partial videos for early predictions. Besides, we utilize the advantages of relational modeling of GNNs to model ASCK among partial videos with arbitrary progress levels. Furthermore, graph generation is the key to building teacher and student networks. In the following subsections, we show graph generation, two backbone layers, the network structure, and our distillation loss.

#### 3.2.1 Graph generation

Consistent with prior works [7], [8], [9], we assume that full videos contain complete action execution, that is to say, the full videos implicitly include partial videos with arbitrary progress levels. Similarly, current partial videos contain other partial videos with lower progress levels. Based on the observation above, the original partial or full videos can be partitioned into a new series of partial videos with lower progress levels. In this way, we can explicitly model ASCK of partial videos with different progress levels for predictions.

Generally, the teacher network is applied to full videos, and the student network is applied to partial videos with different progress levels. Therefore, we build a bi-directional fully connected graph for the teacher network, and we build the other single-directional fully connected graph for the student network since future information is not available during the testing phase. In this way, the teacher network models ASCK among partial videos with arbitrary progress levels. The student network models the ASCK among partial videos from lower progress levels to higher progress levels. As a result, we build two graphs for the teacher and student networks as follows.

As shown in Fig. 4, firstly, we partition the original video  $X$  to obtain new partial videos with different progress levels as defined in section 3.1. Then, we extract two-stream features for representing the partial videos, including RGB features and flow features. Finally, using RGB or flow features of partial videos as nodes and their semantic consistencies as edges, two types of graphs are defined for the teacher and student networks, respectively.

Feature extraction. Two-stream networks have shown great success in a variety of visual tasks [1], [40]. In this

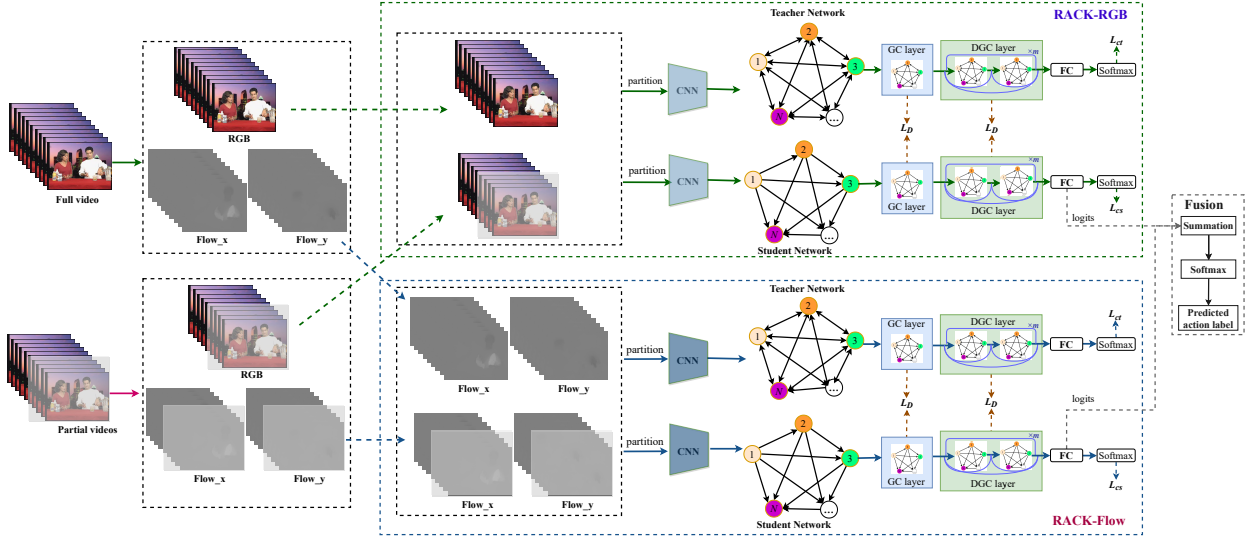


Fig. 3. Overall framework. A novel RACK network is built under the teacher-student framework for early action prediction.

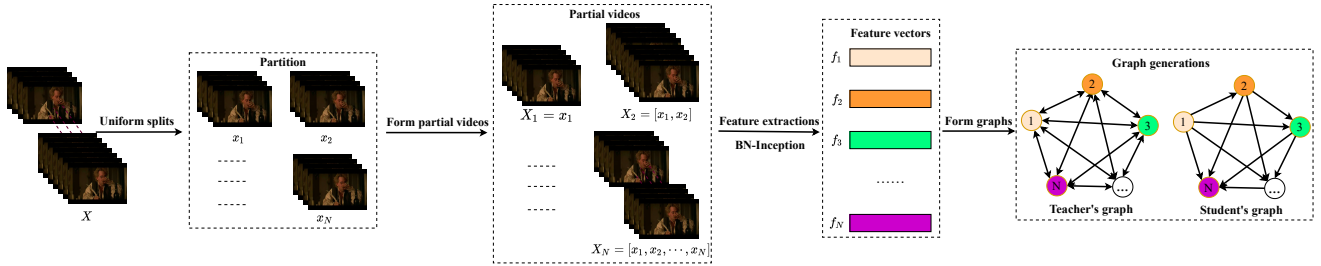


Fig. 4. Graph generation. Given a video  $X$ , we first uniformly split it into  $N$  segments  $\{x_1, x_2, \dots, x_N\}$ . Then, the partial video  $X_n$  with a progress level of  $n$  can be formed by the first  $n$  segments via concatenation along the temporal dimension. Next, we calculate the optical flow of partial videos [40] and apply BN-Inception network [41] to extract their spatiotemporal features using their optical flow images, respectively.  $f_n$  denotes the extracted features of the partial video  $X_n$  ( $n = 1, 2, \dots, N$ ). Finally, two types of graphs are built for the teacher and student networks with the features of partial videos as nodes and their semantic consistencies as edges.

paper, we also follow this pipeline. As described in [42], we also use a pre-trained BN-Inception network [41] on Kinetics-400 dataset [43] to extract the features using RGB and optical flow image sequences of partial or full videos. Taking the optical flow image sequence as an example, we use a sliding window with a size of 5 and an overlap of 4 to collect a batch of optical images. The two-directional optical flow images are stacked and resized as a tensor with a size of  $10 \times 224 \times 224$ . These tensors are set as the input of the BN-Inception network, and we obtain a sequence of feature vectors with a size of  $1 \times D$  (Here,  $D=1024$ ) for each partial or full video. Furthermore, we apply an average pooling to these feature vectors and obtain the final feature representation with a size of  $1 \times D$  for a partial or full video. Finally, we extract RGB and flow features of partial or full videos, respectively.

### 3.2.2 Graph convolutional (GC) layer

To model semantic consistencies among partial or full videos, we define a graph convolutional network layer as follows by equation 2.

$$F_{l+1} = GC(F_l) = A_l F_l W_l \quad (2)$$

where  $GC(\cdot)$  denotes the defined graph convolutional layer,  $F_l$  denotes a tensor with a shape of  $N \times D_l$  at the  $l$ -th layer, and the  $i$ -th row of the tensor denotes the feature vector of a partial video with a progress level of  $i$  as described in section 3.2.1.  $W_l$  is a learnable weight with a shape of  $D_l \times D_{l+1}$ , and  $D_l$  is the dimension of the  $l$ -th layer.  $A_l$  denotes the adjacent matrix with a shape of  $N \times N$ , and  $N$  denotes the number of progress levels of partial videos.

Instead of simply initializing the adjacent matrix with random weights as done in prior works [28], we add a constrained matrix to the adjacent matrix by an element-wise multiplication. The constrained matrix is calculated by the cosine similarity between two partial or full videos, encouraging the network to maximize their similarities and model their semantic consistencies. Therefore, our adjacent matrix  $A_l$  can be formulated as follows by equation 3.

$$A_l = M \odot A' \odot S \quad (3)$$

where  $M$  is a binary mask matrix that indicates the indexes of partial videos for distillation.  $A'$  denotes a learnable adjacent matrix as done prior works [28], and  $S$  is a introduced constrained matrix. The shape of  $M$ ,  $A'$  or  $S$  is  $N \times N$ , and  $\odot$  denotes an element-wise multiplication.

The constrained matrix  $S$  is formulated as equation 4.

$$s_{ij} = \frac{f_i f_j^T}{\|f_i\|_2 \|f_j\|_2} \quad (4)$$

where  $s_{ij}$  denotes an element of  $S$  at the  $i$ -th row and  $j$ -th column, which can be calculated by the cosine similarity of partial videos between the  $i$ -th progress level and the  $j$ -th progress level.  $i, j = 1, 2, \dots, N$ .  $f_*$  denotes a feature vector of a partial video with a progress level of  $*$ , i.e., the  $*$ -th low of  $F_l$  in equation 2.  $f^T$  denotes the transpose of matrix  $f$ .

### 3.2.3 Densely graph convolutional block (DGC)

To improve the ability of the model, we build a dense graph convolutional block using the predefined GC layer, formulated by equation 5.

$$\begin{aligned} F_{l+1} &= DGC(F_l) \\ &= g(g(F_l) + F_l) + (g(F_l) + F_l) + F_l \end{aligned} \quad (5)$$

where  $g(\cdot)$  denotes a graph convolutional layer  $GC(\cdot)$  followed by a batch normalization layer  $BN(\cdot)$ , a ReLU layer and a dropout layer  $\delta(\cdot)$ , i.e.,  $g(*) = \delta(BN(GC(*)))$ .

The dense connections enable the network to fuse the low-level features from shallow layers via element-wise summation, enhancing the features of each partial video to some extent.

### 3.2.4 Network structure

Based on the generated graphs and the predefined backbone layers, we build our RACK network by the teacher-student framework and the two-stream framework for EAP, including RACK-RGB, RACK-Flow, and fusion module. As shown in Fig. 3, the RACK-RGB and RACK-Flow share the same structure, which takes RGB and flow features as the inputs, respectively. The fusion module obtains the final predictions via summarization logits of RACK-RGB and RACK-Flow sub-networks. The RACK-RGB or RACK-Flow contains a teacher network and a student network. Below, we first show the detailed structures of teacher and student networks and the fusion module. Then, we discuss the rich action-semantic consistent knowledge of the proposed method.

**Teacher network.** We build a bi-directional action-semantic graph for the teacher network as described in Section 3.2.1. More specifically, the element values of binary mask matrix  $M$  in equation 3 are set to 1, i.e.  $m_{ij}=1$ ,  $m_{ij} \in M$  and  $i, j = 1, 2, \dots, N$ . In this way, the teacher network models ASCK among any partial or full videos from lower to higher progress levels and higher to lower progress levels.

The detailed structure of the teacher network is shown in Fig. 3, including a GC layer,  $m$  stacked DGC layers, a fully connected (FC) layer, and a softmax layer, among which the GC and DGC layers are first applied to update the features of nodes and edges of the graph, so as to model the ASCK among different videos with arbitrary progress levels. Then, the FC and softmax layers are applied to obtain the semantic labels of videos.

**Student network.** The student network shares the same structure as the teacher network except for the single-directional action-semantic graph. Therefore, the binary mask matrix  $M$  in equation 3 is defined by equation 6. In

this way, the partial video can not obtain the information from the following partial videos with higher progress levels. The ASCK is modeled among partial videos from lower to higher progress levels. Nonetheless, the distillation loss also distills the ASCK from higher to lower progress levels from the teacher to the student network.

$$m_{ij} = \begin{cases} 1, & i \geq j \\ 0, & \text{otherwise} \end{cases} \quad (6)$$

where  $m_{ij} \in M$  and  $i, j = 1, 2, \dots, N$ .

Furthermore, the FC and softmax layer of the student model are shared with that of the teacher network, which jointly trains the classifiers for EAP.

**Fusion.** Given the logits of partial video  $X_i$  after FC layers of RACK-RGB and RACK-Flow, denoting by  $l_{ir}$  and  $l_{if}$  ( $i = 1, 2, \dots, N$ ), we obtain the final prediction via element-wise summation of the logits and a softmax layer by equation 7.

$$\hat{y}_i = \text{softmax}(l_{ir} \odot l_{if}) \quad (7)$$

where  $\hat{y}_i$  is the predicted label of partial videos.  $l_{ir}$  and  $l_{if}$  are logits of the student network from RACK-RGB and RACK-Flow, respectively.  $\odot$  is an element-wise summation.  $\text{softmax}(\cdot)$  is a softmax layer.

### Rich action-semantic consistent knowledge modeling.

As discussed above, the proposed RACK network models rich action-semantic consistent knowledge from two-fold: (1) graph reasoning-based action-semantic consistent knowledge modeling. Based on the defined action-semantic graphs and graph backbone layers in sections 3.2.1, 3.2.2 and 3.2.3, we model rich action-semantic consistent knowledge among different partial videos via the teacher and student networks. Specifically, the bi-directional semantic graph of the teacher network models rich action-semantic consistent knowledge among arbitrary partial videos that are partitioned from the full videos. The single-directional semantic graph of the student network models action-semantic consistent knowledge of partial videos from lower to higher observation ratios. With these elegant designs, the teacher network obtains complete action-semantic consistent knowledge, and for the student network, the partial videos can utilize the action-semantic consistent knowledge from partial videos with lower observation ratios to improve their semantic predictions. (2) Distillation framework-based action-semantic consistent knowledge modeling. Under the knowledge distillation framework, the action knowledge of partial videos is further enriched by distilling complete action-semantic consistent knowledge from the teacher to the student. To summarize, we model rich action-semantic knowledge for accurate predictions via graph reasoning and knowledge distillation framework.

### 3.2.5 Loss

As shown in Fig. 3, we first train RACK-RGB and RACK-Flow sub-networks separately. Then, we obtain final predictions via the fusion module. The RACK-RGB and RACK-Flow share the same structure and loss. Tanking an example of RACK-RGB, we optimize our model using the loss defined in equation 8, which jointly achieves ASCK distillation and early action-semantic predictions.

$$L = L_D + L_C \tag{8}$$

$$L_D = L_{MSE} + L_{MMD} \\ = \sum_{l=1}^M (\|F_{ls} - F_{lt}\|_2 + \|F_{ls}F_{ls}^T - F_{lt}F_{lt}^T\|) \tag{9}$$

$$L_C = L_{CT} + L_{CS} \\ = \sum_{i=1}^N (CE(\hat{y}_{it}, y_i) + CE(\hat{y}_{is}, y_i)) \tag{10}$$

where  $L_D$  denotes the layer-wise knowledge distillation loss built with MSE and MMD as done in [8].  $L_C$  denotes the overall classification loss, including a classification loss of the teacher network  $L_{CT}$  and a classification loss of the student network  $L_{CS}$ .  $CE(\cdot)$  denotes the standard cross-entropy loss between the prediction  $\hat{y}_{i*}$  and the groundtruth  $y_i$ , where  $\hat{y}_{is}$  and  $\hat{y}_{it}$  are predictions of the student or teacher network, respectively.

## 4 EXPERIMENTS

### 4.1 Datasets and Implementation Details

**Datasets.** (1) UCF101 [44]. UCF101 dataset is collected from YouTube websites in unconstrained environments. It consists of 13320 videos with 101 action classes, including 23 hours of videos. (2) HMDB51 [45]. HMDB51 dataset contains  $\approx 7000$  videos collected from various sources, from movies to YouTube websites. It consists of 51 action classes, and each class has at least 101 videos. (3) Something-Something V2 (Sth-v2) [46]. The Sth-v2 dataset is a large-scale crowd-sourced dataset containing rich human-object interactions. The dataset contains 174 categories and 220847 videos, among which 168913 videos are for the training set, 24777 videos are for the validation set, and 27157 videos are for the testing set. Since the testing set has no label, we use the validation set for reported results. Each video contains 2~6 seconds, and their frame rates are 12 fps/s.

**Implementation Details.** We implement our models using PyTorch [47], and we use SGD [48] with a momentum rate of 0.9 to optimize our models on one GTX 3080Ti GPU. We train 800 epochs on UCF101, 400 epochs on HMDB51, and 1000 epochs on Sth-v2 to choose the best model by the mean accuracy across different progress levels. The learning rate is initialized to 0.00001 and is reduced by a multiplier of 0.95 at the 100-th, 150-th, 250-th, and 350-th epochs, respectively. The batch size is set to 16 on UCF101 and HMDB51 and 256 on Sth-v2. The dropout ratio is set to 0.5. The channels are set to 512 at the GC and DGC layers. Consistent with the baselines, we use the same training or testing splits on UCF101, HMDB51, and Sth-v2 for evaluations. For a fair comparison, we strictly reproduce the results of PTS' in section 4.3 according to the paper in [8] using our features except for their optimized strategies and the weights  $w$  in their KD loss since these items have a limited effect on UCF101. The area under the curve (AUC) is used as our metric by average accuracies over different progress levels, and  $N$  is set to 10 in experiments. The number of stacked DGC layers (i.e.,  $m$ ) is set to 1 on UCF101 and HMDB51 datasets and 2 on the Sth-v2 dataset.

### 4.2 Baselines

To show the effectiveness of our method, we choose several related methods as our baselines, including three traditional methods, i.e., IBOW [49], DBOW [49], MTSSVM [50], and five methods based on deep neural networks, i.e., DeepSCN [21], Mem-LSTM [12], MSRNN [9], PTS [8] AKT [7], AAPNet [51], AJSM [22], and AFR [52], among which AKT [7], PTS [8], AAPNet [51], AJSM [22], and AFR [52] achieve current state-of-the-art performance.

### 4.3 Comparison with baselines

#### 4.3.1 Prediction results on UCF101

As shown in Table 1, our method consistently outperforms all baselines in terms of AUC. Moreover, our results of single-mode features (i.e., Ours-RGB or Ours-Flow) have exceeded most baselines, showing the effectiveness of our method.

Compared with the traditional methods with hand-crafted features [49], [50], we obtain a significantly improved accuracy by a margin of at least 17.84%, demonstrating the effectiveness of our method powerfully. Compared with some typical methods with deep features [9], [12], [21], we also achieve an appreciable performance by a margin of at least 8.00%. Moreover, Mem-LSTM [12] and MSRNN [9] use two-stream features and pre-train their models on UCF101, which enables their models to obtain the domain action knowledge on UCF101. By contrast, we extract features of partial or full videos by the pre-trained model on Kinetics-400 without fine-tuning on UCF101. In this way, we can not obtain domain-specific knowledge. Nevertheless, we still achieve improved accuracy by an appreciable margin, showing the effectiveness of our method again.

Compared with other recent methods [7], [8], [22], [51], [52], we also achieve the best performance in terms of AUC. PTS [8] distills progressive action knowledge between adjacent partial videos. AKT [7], AJSM [22] and AAPNet [51] transfer action knowledge from full videos to partial videos by learning the feature embeddings and discriminative action classifiers. AFR [52] models spatial and temporal interactions among objects and synthesizes their future spatio-temporal relationships. However, PTS [8] ignores the correlations of partial videos between lower observation ratios and higher observation ratios. AKT [7], AJSM [22], AAPNet [51] and AFR [52] ignore the correlations among partial videos with different progress levels, leading to their unsatisfactory performance.

We often ignore the phenomenon that any partial or full video usually contains other partial videos with lower observation ratios than itself. Based on the observations, we model rich ASCK among arbitrary partial or full videos via graph-based knowledge reasoning and knowledge distillation framework. For the graph-based knowledge reasoning, we distill ASCK among partial videos from lower progress levels to higher progress levels and higher progress levels to lower progress levels by the teacher network; we also distill ASCK of partial videos from lower progress levels to higher progress levels by the student network since future information is not available at the test phase. Under the knowledge distillation framework, we further transfer action knowledge from the teacher network to the student

TABLE 1

Quantitative results on UCF101. The results for DBOW [49], IBOW [49], MTSSVM [50], DeepSCN [21], Mem-LSTM [12], MSRNN [9] and PTS [8] are reported in [8]. The corresponding results of AKT [7] are also reported in their paper. For a fair comparison, we also reproduce the results of PTS [8] using the extracted feature in the paper, and we name it PTS'. "Ours-RGB" and "Ours-Flow" report the results of "RACK-RGB" and "RACK-Flow" sub-networks in Fig. 3, respectively. The bold denotes the best results. - denotes unavailable results.

| Method                   | Features        | Pre-trained data    | Modality | 0.1          | 0.2          | 0.3          | AUC          |
|--------------------------|-----------------|---------------------|----------|--------------|--------------|--------------|--------------|
| DBOW (ICCV2011) [49]     | STIP            | No                  | RGB      | 36.29        | 51.57        | 52.71        | 51.37        |
| IBOW (ICCV2011) [49]     | STIP            | No                  | RGB      | 36.29        | 65.69        | 71.69        | 70.01        |
| MTSSVM (ACMMM2019) [50]  | STIP+DT         | No                  | RGB      | 40.05        | 72.83        | 80.02        | 77.41        |
| DeepSCN (CVPR2017) [21]  | C3D             | Sports-1M           | RGB      | 45.02        | 77.64        | 82.95        | 81.31        |
| Mem-LSTM (AAAI2018) [12] | ResNet-18       | ImageNet+UCF101     | RGB+Flow | 51.02        | 80.97        | 85.73        | 84.10        |
| MSRNN (TPAMI2018) [9]    | VGG             | UCF101              | RGB+Flow | 68.00        | 87.39        | 88.16        | 87.25        |
| AKT (AAAI2019) [7]       | 3D ResNeXt-101  | Kinetics-400        | RGB      | 80.00        | 84.7         | 86.90        | 88.4         |
| PTS (CVPR2019) [8]       | 3D ResNeXt-101  | Kinetics-400        | RGB      | 83.32        | 87.13        | 88.92        | 89.64        |
| PTS' (CVPR2019) [8]      | BN-Inception    | Kinetics-400        | Flow     | 74.31        | 87.51        | 90.03        | 91.02        |
| AAPNet (TPAMI2020) [51]  | BN-Inception    | Unknown             | RGB+FLOW | 59.84        | 80.44        | 86.78        | 85.13        |
| AJSM (CVPR2021) [22]     | Resnet18(2D+1D) | Kinetics-400        | RGB+FLOW | -            | 91.70        | -            | -            |
| AFR (AAAI2021) [52]      | BN-Inception    | Kinetics-400+UCF101 | RGB+FLOW | 82.36        | 85.57        | 88.97        | -            |
| Ours-RGB                 | BN-Inception    | Kinetics-400        | RGB      | 83.76        | 85.82        | 87.67        | 88.28        |
| Ours-Flow                | BN-Inception    | Kinetics-400        | FLOW     | 73.06        | 86.77        | 90.36        | 91.20        |
| Ours                     | BN-Inception    | Kinetics-400        | RGB+FLOW | <b>90.03</b> | <b>93.64</b> | <b>95.08</b> | <b>95.25</b> |

TABLE 2

Quantitative results on HMDB51. The corresponding results of AKT [7] are also reported in their paper. For a fair comparison, we also reproduce the results of PTS [8] using the extracted features in the paper, and we name it PTS'. "Ours-RGB" and "Ours-Flow" report the results of "RACK-RGB" and "RACK-Flow" sub-networks in Fig. 3, respectively. The bold denotes the best results.

| Method              | Features       | Pre-trained data | Modality | 0.1          | 0.2          | 0.3          | AUC          |
|---------------------|----------------|------------------|----------|--------------|--------------|--------------|--------------|
| AKT (AAAI2019) [7]  | 3D ResNeXt-101 | Kinetics-400     | RGB      | 43.5         | 48.4         | 51.2         | 55.5         |
| PTS' (CVPR2019) [8] | BN-Inception   | Kinetics-400     | Flow     | 41.14        | 50.88        | 56.85        | 62.38        |
| Ours-RGB            | BN-Inception   | Kinetics-400     | RGB      | 46.44        | 50.90        | 54.89        | 57.32        |
| Ours-Flow           | BN-Inception   | Kinetics-400     | FLOW     | 41.18        | 51.39        | 54.93        | 63.85        |
| Ours                | BN-Inception   | Kinetics-400     | RGB+FLOW | <b>53.56</b> | <b>58.92</b> | <b>62.58</b> | <b>68.55</b> |

network, which enriches the ASCK of partial videos for accurate predictions. The above reasons possibly enable our model to achieve superior predictions. We further report detailed results with different observation ratios in Fig. 5. Our method outperforms all baselines at all observation ratios, especially at very low observation ratios, showing our effectiveness again.

#### 4.3.2 Prediction results on HMDB51

Compared with the UCF101 dataset, the HMDB51 dataset is more challenging due to more diverse sources and larger intra-class variances, making it more difficult to predict human action very early. As shown in Table 2, compared with AKT [7] and PTS' [8], we achieve superior performance in terms of AUC by a margin of 13.05% and 6.17%, respectively. Although [7] and [8] try to distill action knowledge from full videos, they ignore ASCK among partial videos with different progress levels, especially the semantic consistencies between higher progress levels and lower progress levels. In contrast, we model rich ASCK among partial videos with richer progress levels via graph-based knowledge reasoning and knowledge distillation framework. The mentioned reason may contribute to our superior predictions on the more challenging dataset, strongly showing the importance of explicitly modeling richer ASCK among partial videos for complex activities.

Fig. 5 shows the detailed results with different observation ratios on HMDB51. We achieve the highest accuracy by

an appreciable margin at all observation ratios. Specifically, compared with AKT [7] and PTS' [8], we have improved accuracy at the progress level of 1 by 10.06% and 12.42%, respectively, and our performance is consistently improved at the following progress levels.

#### 4.3.3 Prediction results on Sth-v2

Unlike UCF101 and HMDB51 datasets that contain rich scene information, the Sth-v2 dataset contains richer motion information, and it is hard to predict human actions according to the scene information. Therefore, predicting human action very early is particularly challenging. It is more important to capture rich action-semantic consistent knowledge for predictions on such a dataset. We use our extracted RGB and flow features and our same fusion strategies to reproduce the results of PTS [8], naming PTS'. Detailed results are shown in Table 3. Compared with PTS', our method consistently outperforms it using the same features in terms of AUC (15.25%vs18.24%, 23.36%vs24.56%, 25.91%vs27.63%). For different observation ratios, we also achieve better results in most cases. For the observation ratio of 0.2, our accuracy is slightly decreased. The possible reason is the limited useful information and low predictability of actions caused by short videos at a very early. At the later observation ratios, we achieve improved performance significantly, showing the effectiveness of our method.

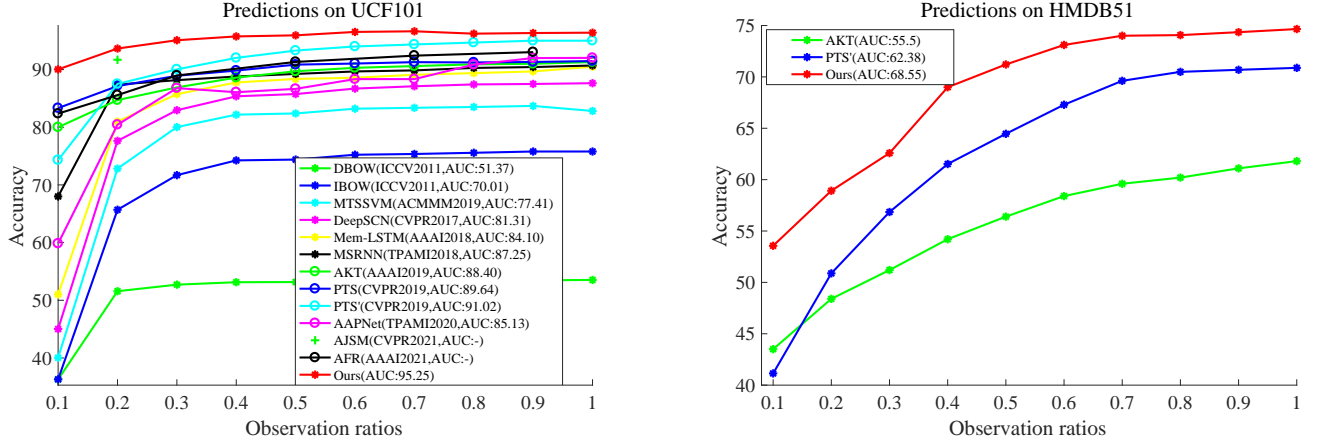


Fig. 5. Prediction results with different observation ratios on UCF101 and HMDB51 datasets. (\*) denotes the performance of the corresponding method in terms of AUC.

TABLE 3

Quantitative results on Sth-v2. For a fair comparison, we also reproduce the results of PTS [8] using our extracted features, and we name it PTS'(\*). "Ours-RGB" and "Ours-Flow" report the results of "RACK-RGB" and "RACK-Flow" sub-networks in Fig. 3, respectively. The bold denotes the best results.

| Method                | Features     | Pre-trained data | Modality | 0.2          | 0.4          | 0.8          | AUC          |
|-----------------------|--------------|------------------|----------|--------------|--------------|--------------|--------------|
| PTS'(1)(CVPR2019) [8] | BN-Inception | Kinetics-400     | RGB      | 11.99        | 14.00        | 17.86        | 15.25        |
| PTS'(2)(CVPR2019) [8] | BN-Inception | Kinetics-400     | FLOW     | 12.89        | 20.31        | 30.80        | 23.36        |
| PTS'(3)(CVPR2019) [8] | BN-Inception | Kinetics-400     | RGB+FLOW | <b>16.92</b> | 23.08        | 32.43        | 25.91        |
| Ours-RGB              | BN-Inception | Kinetics-400     | RGB      | 11.90        | 15.04        | 23.02        | 18.24        |
| Ours-Flow             | BN-Inception | Kinetics-400     | FLOW     | 12.83        | 20.85        | 32.98        | 24.56        |
| Ours                  | BN-Inception | Kinetics-400     | RGB+FLOW | 16.21        | <b>23.67</b> | <b>35.51</b> | <b>27.63</b> |

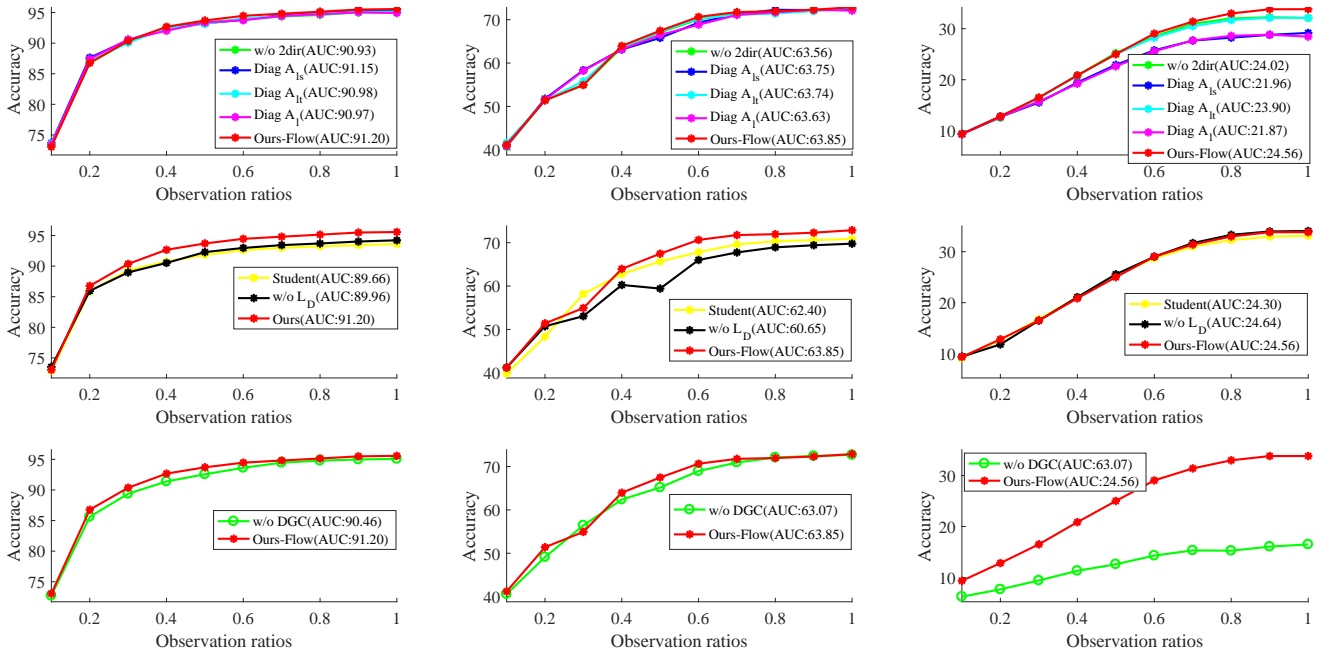


Fig. 6. Detailed results of ablative studies. (\*) denotes the performance of the corresponding method in terms of AUC. The left one denotes the results on UCF101, the middle one denotes the results on HMDB51, and the right one denotes the results on Sth-v2.

#### 4.4 Ablation analysis

In this section, we conduct extensive experiments using flow features to show the effectiveness of our key contributions. Firstly, we show the effectiveness of rich ASCK via

graph-based knowledge reasoning and knowledge distillation framework. Then, we evaluate the rationality of the DGC structure. Finally, we briefly analyze the parameters of our RACK.



TABLE 4  
Parameter analysis. The bold marks the best results. “+\*” denotes the improved results.

| Method    | GPU Memory | GPU Memory | AUC          |              |             |
|-----------|------------|------------|--------------|--------------|-------------|
|           |            |            | UCF101       | HMDB51       | Sth-v2      |
| PTS'      | 3303M      | 5.8M       | 91.02        | 62.38        | 23.36       |
| Ours-Flow | 861M       | 2.2M       | 91.20(+0.18) | 63.85(+1.47) | 24.56(+1.2) |

#### 4.4.1 Evaluation of modeling rich ASCK

Our rich ASCK modeling benefits from two-fold: graph-based knowledge reasoning, and knowledge distillation framework.

**Effectiveness of graph-based knowledge reasoning.** We conduct four group experiments to show the effectiveness of graph-based knowledge reasoning. (1) Change the bi-directional graph of the teacher network into a single directional graph, denoting by “w/o 2dir”. In this way, the teacher network models action knowledge from lower to higher progress levels. (2) Setting the adjacent matrix of the teacher network to a diagonal matrix. In this way, the teacher network ignores modeling ASCK of different progress levels, denoting by “Diag  $A_{lt}$ ”. (3) Setting the adjacent matrix of the student network to a diagonal matrix. In this way, the student network ignores modeling ASCK of different progress levels, denoting by “Diag  $A_{ls}$ ”. (4) Setting the adjacent matrix of the teacher and student networks to a diagonal matrix. In this way, the teacher and student networks ignore modeling ASCK of different progress levels, denoting by “Diag  $A_l$ ”.

As shown in Table 5, the top ones show the effectiveness of distilling ASCK via graph-based knowledge reasoning. Compared with “Ours-Flow”, the AUC of “w/o 2dir” decreases by 0.27%, 0.29% and 0.54% on UCF101, HMDB51, and Sth-v2, respectively. The single-directional graph by the teacher network still enables the model to distill ASCK from lower to higher progress levels. Therefore, the teacher network with the single-directional graph also greatly helps to improve the predictions. When we do not consider the ASCK of the teacher or student network by setting the adjacent matrixes to the diagonal matrixes (i.e., “Diag  $A_{ls}$ ”, “Diag  $A_{lt}$ ”, and “Diag  $A_l$ ”), the performance consistently decreases, especially on the motion dataset (i.e., Sth-v2), showing the effectiveness of rich ASCK via graph-based knowledge reasoning.

**Effectiveness of knowledge distillation framework.** We conduct two group experiments to show the effectiveness of modeling rich ASCK via the knowledge distillation framework. (1) Removing the teacher network, denoting by “Student”. In this way, our model ignores the ASCK from the full videos. (2) Removing the feature-level distillation loss  $L_D$  in equation 7, denoting by “w/o  $L_D$ ”. In this way, our model will ignore learning feature-level ASCK from the teacher to the student network.

Detailed results are shown in Table 5. Without considering the ASCK from the teacher network (“Student”), the AUC decreases by 1.54%, 1.45%, and 0.26% on UCF101, HMDB51, and Sth-v2, respectively. Compared with “Ours-Flow”, the AUC of “w/o  $L_D$ ” also decreases by 1.24% and 3.2% on UCF101, HMDB51, and Sth-v2, respectively. These results prove the effectiveness of rich action knowledge

TABLE 5

Results of ablative studies. The bold marks the best results, “(-)” shows the decreased accuracy compared with our results, and the AUC denotes the average prediction overall ten progress levels.

| Model         | AUC          |              |                     |
|---------------|--------------|--------------|---------------------|
|               | UCF101       | HMDB51       | Sth-v2              |
| w/o 2dir      | 90.93(-0.27) | 63.56(-0.29) | 24.02(-0.54)        |
| Diag $A_{ls}$ | 91.15(-0.05) | 63.75(-0.10) | 21.96(-2.60)        |
| Diag $A_{lt}$ | 90.98(-0.22) | 63.74(-0.11) | 23.90(-0.66)        |
| Diag $A_l$    | 90.97(-0.23) | 63.63(-0.22) | 21.87(-2.69)        |
| Student       | 89.66(-1.54) | 62.40(-1.45) | 24.30(-0.26)        |
| w/o $L_D$     | 89.96(-1.24) | 60.65(-3.2)  | <b>24.64(+0.08)</b> |
| w/o DC        | 90.46(-0.74) | 63.07(-0.78) | 12.47(-12.09)       |
| Ours-Flow     | <b>91.20</b> | <b>63.85</b> | 24.56               |

modeling via a knowledge distillation framework, especially on scene-related datasets (i.e., UCF101 and HMDB51).

Fig. 6 shows the detailed results with different progress levels on UCF101, HMDB51, and Sth-v2. The improved results on various datasets show the effectiveness of our rich ASCK modeling via graph-based knowledge reasoning and a knowledge distillation framework. Comparing their results, we make two interesting conclusions. (1) It is more effective to model rich ASCK via a knowledge distillation framework for the predictions on the scene-related datasets (i.e., UCF101 and HMDB51); (2) while it is more effective to model rich ASCK via a graph-based knowledge reasoning for the predictions on the motion-related dataset (i.e., Sth-v2).

#### 4.4.2 Evaluation of the rationality of DGC structure

“w/o DC” denotes without densely residual connections in the DGC block. As shown in Table 5, compared with “w/o DC”, the accuracy of our method increases by 0.74%, 0.78%, and 12.09% on UCF101, HMDB51, and Sth-v2, respectively. The results show the effectiveness of the densely residual connections in leveraging low-level features for accurate predictions, especially on the challenging dataset that contains rich motion information. The detailed results in Fig. 6 also show similar improved results. Therefore, the results in Table 5 and Fig. 6 consistently show the rationality of DGC structure.

### 4.5 Visualization

To further show the effectiveness of our proposed RACK network, we visualize our learned features using t-SNE technique [53]. Taking an example of flow modality on the UCF101 dataset, we treat the extracted features of partial videos in section 3.2.1 as the original features, and we treat the features before the FC layer of the student network at the RACK-Flow in Fig. 3 as our learned features. As shown

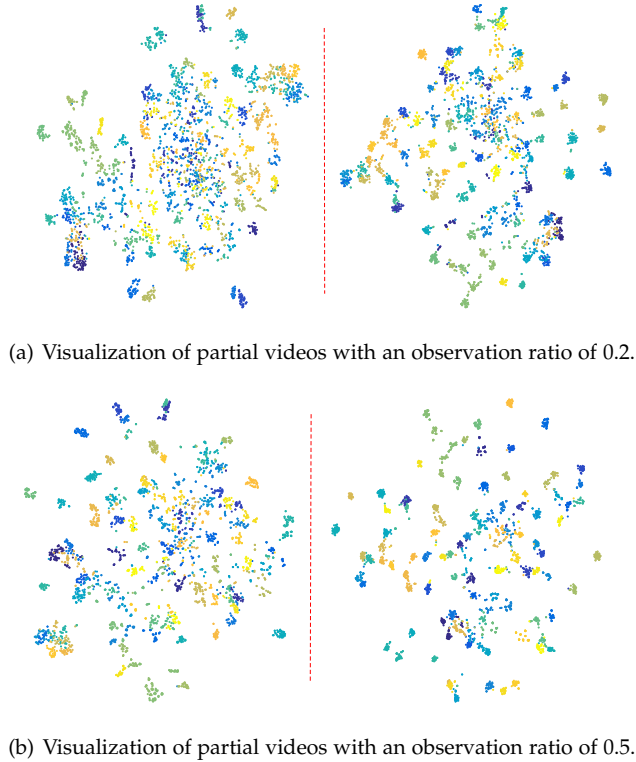


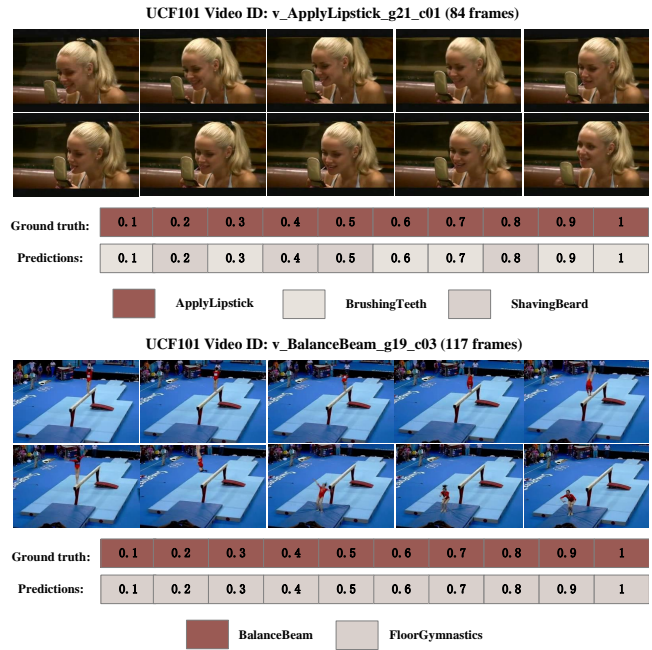
Fig. 7. t-SNE [53] visualization of flow features on UCF101. The left one denotes the visualization of extracted initially flow features. The right one indicates the visualization of our learned features, i.e., the features before the FC layer of RACK-Flow in Fig. 3.

in Fig. 7, we visualize the features of partial videos with an observation ratio of 0.2 and 0.5, respectively. The visualizations show that our learned features can be grouped better, indicating the effectiveness of rich action-semantic consistent knowledge modeling by our proposed RACK network.

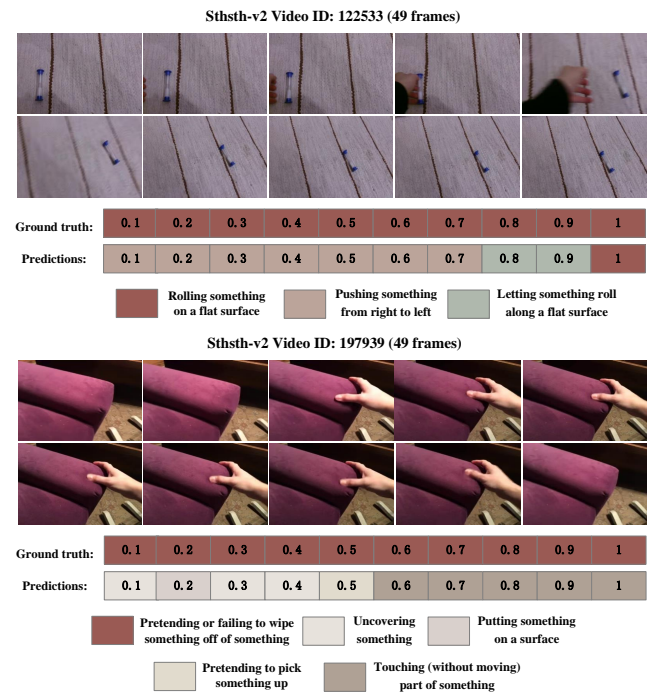
#### 4.6 Failed cases analysis

To reveal the limitation of our proposed method, we visualize some failed predictions on UCF101 and Sthst-v2 datasets, as shown in Fig. 8. The failed cases on UCF101 are shown in Fig. 8(a). (1) “ApplyLipstick” is easily predicted as “BrushingTeeth” and “ShavingBeard”. Two main reasons may lead to the failed results. One is similar spatio-temporal semantics of these activities. The other is short durations of full videos that may lead to extremely limited action information of partial videos. (2) “BalanceBeam” is incorrectly predicted as “FloorGymnastics”. The possible reason is that the human body movements of “BalanceBeam” and “FloorGymnastics” are very similar. They need to be combined with a strong scene context before better distinguishing. However, we find that the scene context of “BalanceBeam” and “FloorGymnastics” are usually confused on the training set. These reasons may lead to incorrect predictions about the two activities.

As shown in Fig. 8(b), the failed cases on Sthst-v2 are similar to that on UCF101, and they are usually misjudged as activities with similar spatio-temporal semantics and short durations. Another important reason is that the pre-trained



(a) Failed results on UCF101.



(b) Failed results on Sthst-v2.

Fig. 8. Visualization of failed predictions. The selected images are uniformly sampled from original videos. The boxes in different colors denote the predictions or Ground truth.

Kinetics-400 dataset is a scene context-related dataset, while Sthst-v2 is a motion dataset. This may lead to the domain gap between different datasets (scene dataset *vs* motion dataset) and various tasks (action recognition *vs* action prediction). Therefore, the extracted features may not sufficiently represent the actions Sthst-v2 dataset and have poor predictive ability, especially for these highly similar activities.

In summary, although our proposed method has achieved a promising performance on multiple diverse datasets, there are some limitations on incorrect predictions on the activities with complex coupled backgrounds, extremely short durations, and highly similar action spatio-temporal semantics. In the future, we will explore a domain feature representation and a hierarchical prediction scheme for these similar activities.

## 5 CONCLUSION

In this paper, we propose a novel RACK network under a teacher-student framework, mining rich ASCK of partial videos with arbitrary progress levels utilizing the graph-based knowledge reasoning and knowledge distillation framework. Specifically, we build a bi-directional and a single-directional fully connected graph for the teacher and student networks, respectively. The teacher network with the bi-directional graph considers ASCK of partial videos with arbitrary progress levels. The student network with the single-directional graph captures ASCK among partial videos from lower to higher progress levels. Also, it enriches their ASCK from the teacher network via distillation loss. In contrast to prior works, we model rich ASCK among arbitrary partial videos and distill ASCK by graph-based knowledge reasoning and the teacher-student framework. Extensive experiments have shown the effectiveness of explicitly modeling rich ASCK for predictions. However, the proposed method fails to predict similar activities with short durations and confusing backgrounds. We will explore a deeper investigation in the future.

## ACKNOWLEDGMENTS

This work was supported partly by the National Natural Science Foundation of China (Grant No. 62173045, 61673192), partly supported by the Fundamental Research Funds for the Central Universities(Grant No. 2020XD-A04-2), and partly supported by BUPT Excellent Ph.D. Students Foundation (CX2021314).

## REFERENCES

- [1] H. Zhao and R. P. Wildes, "Review of video predictive understanding: Early action recognition and future action prediction," *arXiv preprint arXiv:2107.05140*, 2021.
- [2] Y. Kong and Y. Fu, "Human action recognition and prediction: A survey," *arXiv preprint arXiv:1806.11230*, 2018.
- [3] L. Chen, J. Lu, Z. Song, and J. Zhou, "Part-activated deep reinforcement learning for action prediction," in *Proceedings of the European Conference on Computer Vision (ECCV)*, 2018, pp. 421–436.
- [4] C. Sun, A. Shrivastava, C. Vondrick, R. Sukthankar, K. Murphy, and C. Schmid, "Relational action forecasting," in *Proceedings of the IEEE Conference on Computer Vision and Pattern Recognition (CVPR)*, 2019, pp. 273–283.
- [5] J. Liu, A. Shahroudy, G. Wang, L.-Y. Duan, and A. C. Kot, "Ss-net: scale selection network for online 3d action prediction," in *Proceedings of the IEEE Conference on Computer Vision and Pattern Recognition (CVPR)*, 2018, pp. 8349–8358.
- [6] H. Gammulle, S. Denman, S. Sridharan, and C. Fookes, "Predicting the future: A jointly learnt model for action anticipation," in *Proceedings of the IEEE International Conference on Computer Vision (ICCV)*, 2019, pp. 5562–5571.
- [7] Y. Cai, H. Li, J.-F. Hu, and W.-S. Zheng, "Action knowledge transfer for action prediction with partial videos," in *Proceedings of the AAAI Conference on Artificial Intelligence (AAAI)*, vol. 33, no. 01, 2019, pp. 8118–8125.
- [8] X. Wang, J.-F. Hu, J.-H. Lai, J. Zhang, and W.-S. Zheng, "Progressive teacher-student learning for early action prediction," in *Proceedings of the IEEE Conference on Computer Vision and Pattern Recognition (CVPR)*, 2019, pp. 3556–3565.
- [9] J.-F. Hu, W.-S. Zheng, L. Ma, G. Wang, J. Lai, and J. Zhang, "Early action prediction by soft regression," *IEEE Transactions on Pattern Analysis and Machine Intelligence (TPAMI)*, vol. 41, no. 11, pp. 2568–2583, 2018.
- [10] S. Lai, W.-S. Zheng, J.-F. Hu, and J. Zhang, "Global-local temporal saliency action prediction," *IEEE Transactions on Image Processing (TIP)*, vol. 27, no. 5, pp. 2272–2285, 2017.
- [11] Q. Ke, M. Bennamoun, H. Rahmani, S. An, F. Sohel, and F. Bousaid, "Learning latent global network for skeleton-based action prediction," *IEEE Transactions on Image Processing (TIP)*, vol. 29, pp. 959–970, 2019.
- [12] Y. Kong, S. Gao, B. Sun, and Y. Fu, "Action prediction from videos via memorizing hard-to-predict samples," in *Proceedings of the AAAI Conference on Artificial Intelligence (AAAI)*, vol. 32, no. 1, 2018.
- [13] T. Li, J. Liu, W. Zhang, and L. Duan, "Hard-net: Hardness-aware discrimination network for 3d early activity prediction," in *Proceedings of the European Conference on Computer Vision (ECCV)*. Springer, 2020, pp. 420–436.
- [14] X. Wu, R. Wang, J. Hou, H. Lin, and J. Luo, "Spatial-temporal relation reasoning for action prediction in videos," *International Journal of Computer Vision (IJCV)*, vol. 129, no. 5, pp. 1484–1505, 2021.
- [15] T. Yao, M. Wang, B. Ni, H. Wei, and X. Yang, "Multiple granularity group interaction prediction," in *Proceedings of the IEEE Conference on Computer Vision and Pattern Recognition (CVPR)*, 2018, pp. 2246–2254.
- [16] K. Li, J. Hu, and Y. Fu, "Modeling complex temporal composition of actionlets for activity prediction," in *Proceedings of the European Conference on Computer Vision (ECCV)*. Springer, 2012, pp. 286–299.
- [17] K. Li and Y. Fu, "Prediction of human activity by discovering temporal sequence patterns," *IEEE Transactions on Pattern Analysis and Machine Intelligence (TPAMI)*, vol. 36, no. 8, pp. 1644–1657, 2014.
- [18] Y. Shi, B. Fernando, and R. Hartley, "Action anticipation with rbf kernelized feature mapping rnn," in *Proceedings of the European Conference on Computer Vision (ECCV)*, 2018, pp. 301–317.
- [19] Z. Xu, L. Qing, and J. Miao, "Activity auto-completion: Predicting human activities from partial videos," in *Proceedings of the IEEE International Conference on Computer Vision (ICCV)*, 2015, pp. 3191–3199.
- [20] Y. B. Ng and B. Fernando, "Forecasting future action sequences with attention: a new approach to weakly supervised action forecasting," *IEEE Transactions on Image Processing (TIP)*, vol. 29, pp. 8880–8891, 2020.
- [21] Y. Kong, Z. Tao, and Y. Fu, "Deep sequential context networks for action prediction," in *Proceedings of the IEEE Conference on Computer Vision and Pattern Recognition (CVPR)*, 2017, pp. 1473–1481.
- [22] B. Fernando and S. Herath, "Anticipating human actions by correlating past with the future with jaccard similarity measures," in *Proceedings of the IEEE Conference on Computer Vision and Pattern Recognition (CVPR)*, 2021, pp. 13 224–13 233.
- [23] G. Pang, X. Wang, J. Hu, Q. Zhang, and W.-S. Zheng, "Dbdnet: Learning bi-directional dynamics for early action prediction," in *International Joint Conference on Artificial Intelligence (IJCAI)*, 2019, pp. 897–903.
- [24] J. Guan, Y. Yuan, K. M. Kitani, and N. Rhinehart, "Generative hybrid representations for activity forecasting with no-regret learning," in *Proceedings of the IEEE Conference on Computer Vision and Pattern Recognition (CVPR)*, 2020, pp. 173–182.
- [25] Z. Wu, S. Pan, F. Chen, G. Long, C. Zhang, and S. Y. Philip, "A comprehensive survey on graph neural networks," *IEEE Transactions on Neural Networks and Learning Systems (TNNLS)*, vol. 32, no. 1, pp. 4–24, 2020.
- [26] S. Yan, Y. Xiong, and D. Lin, "Spatial temporal graph convolutional networks for skeleton-based action recognition," in *The AAAI Conference on Artificial Intelligence (AAAI)*, 2018.
- [27] K. Cheng, Y. Zhang, X. He, W. Chen, J. Cheng, and H. Lu, "Skeleton-based action recognition with shift graph convolutional network," in *Proceedings of the IEEE Conference on Computer Vision and Pattern Recognition (CVPR)*, 2020, pp. 183–192.
- [28] W. Mao, M. Liu, M. Salzmann, and H. Li, "Learning trajectory dependencies for human motion prediction," in *Proceedings of the*

- IEEE International Conference on Computer Vision (ICCV)*, 2019, pp. 9489–9497.
- [29] Y. Chen, M. Rohrbach, Z. Yan, Y. Shuicheng, J. Feng, and Y. Kalantidis, “Graph-based global reasoning networks,” in *Proceedings of the IEEE Conference on Computer Vision and Pattern Recognition (CVPR)*, 2019, pp. 433–442.
- [30] X. Wang and A. Gupta, “Videos as space-time region graphs,” in *Proceedings of the European Conference on Computer Vision (ECCV)*, 2018, pp. 399–417.
- [31] Y. Yuan, X. Liang, X. Wang, D.-Y. Yeung, and A. Gupta, “Temporal dynamic graph lstm for action-driven video object detection,” in *Proceedings of the IEEE International Conference on Computer Vision (ICCV)*, 2017, pp. 1801–1810.
- [32] X. Liu, J.-Y. Lee, and H. Jin, “Learning video representations from correspondence proposals,” in *Proceedings of the IEEE Conference on Computer Vision and Pattern Recognition (CVPR)*, 2019, pp. 4273–4281.
- [33] C. Zhao, A. K. Thabet, and B. Ghanem, “Video self-stitching graph network for temporal action localization,” in *Proceedings of the IEEE International Conference on Computer Vision (ICCV)*, 2021, pp. 13 658–13 667.
- [34] M. Xu, C. Zhao, D. S. Rojas, A. Thabet, and B. Ghanem, “G-tad: Sub-graph localization for temporal action detection,” in *Proceedings of the IEEE Conference on Computer Vision and Pattern Recognition (CVPR)*, 2020, pp. 10 156–10 165.
- [35] R. Zeng, W. Huang, M. Tan, Y. Rong, P. Zhao, J. Huang, and C. Gan, “Graph convolutional networks for temporal action localization,” in *Proceedings of the IEEE International Conference on Computer Vision (ICCV)*, 2019, pp. 7094–7103.
- [36] Y. Bai, Y. Wang, Y. Tong, Y. Yang, Q. Liu, and J. Liu, “Boundary content graph neural network for temporal action proposal generation,” in *Proceedings of the European Conference on Computer Vision (ECCV)*. Springer, 2020, pp. 121–137.
- [37] R.-C. Li, T. Xu, X.-J. Wu, and J. Kittler, “Video is graph: Structured graph module for video action recognition,” *arXiv preprint arXiv:2110.05904*, 2021.
- [38] J. Gou, B. Yu, S. J. Maybank, and D. Tao, “Knowledge distillation: A survey,” *International Journal of Computer Vision (IJCV)*, vol. 129, no. 6, pp. 1789–1819, 2021.
- [39] G. Hinton, O. Vinyals, and J. Dean, “Distilling the knowledge in a neural network,” *arXiv preprint arXiv:1503.02531*, 2015.
- [40] L. Wang, Y. Xiong, Z. Wang, Y. Qiao, D. Lin, X. Tang, and L. Van Gool, “Temporal segment networks: Towards good practices for deep action recognition,” in *Proceedings of the European Conference on Computer Vision (ECCV)*. Springer, 2016, pp. 20–36.
- [41] S. Ioffe and C. Szegedy, “Batch normalization: Accelerating deep network training by reducing internal covariate shift,” in *International Conference on Machine Learning (ICML)*. PMLR, 2015, pp. 448–456.
- [42] J. Yin, X. Liu, F. Sun, H. Liu, Z. Liu, B. Wang, J. Liu, and Y. Yin, “One-shot sadi-epe: a visual framework of event progress estimation,” *IEEE Transactions on Circuits and Systems for Video Technology (TCSVT)*, vol. 29, no. 6, pp. 1659–1671, 2018.
- [43] W. Kay, J. Carreira, K. Simonyan, B. Zhang, C. Hillier, S. Vijayanarasimhan, F. Viola, T. Green, T. Back, P. Natsev *et al.*, “The kinetics human action video dataset,” *arXiv preprint arXiv:1705.06950*, 2017.
- [44] K. Soomro, A. R. Zamir, and M. Shah, “Ucf101: A dataset of 101 human actions classes from videos in the wild,” *arXiv preprint arXiv:1212.0402*, 2012.
- [45] H. Kuehne, H. Jhuang, E. Garrote, T. Poggio, and T. Serre, “Hmdb: a large video database for human motion recognition,” in *Proceedings of the IEEE International Conference on Computer Vision (ICCV)*. IEEE, 2011, pp. 2556–2563.
- [46] J. Materzynska, T. Xiao, R. Herzig, H. Xu, X. Wang, and T. Darrell, “Something-else: Compositional action recognition with spatial-temporal interaction networks,” in *Proceedings of the IEEE/CVF Conference on Computer Vision and Pattern Recognition*, 2020, pp. 1049–1059.
- [47] A. Paszke, S. Gross, S. Chintala, G. Chanan, E. Yang, Z. DeVito, Z. Lin, A. Desmaison, L. Antiga, and A. Lerer, “Automatic differentiation in pytorch,” in *Workshop on Neural Information Processing Systems (NIPS-W)*, 2017.
- [48] L. Bottou, “Large-scale machine learning with stochastic gradient descent,” in *Proceedings of COMPSTAT 2010*. Springer, 2010, pp. 177–186.
- [49] M. S. Ryoo, “Human activity prediction: Early recognition of ongoing activities from streaming videos,” in *Proceedings of the IEEE International Conference on Computer Vision (ICCV)*. IEEE, 2011, pp. 1036–1043.
- [50] W. Xu, J. Yu, Z. Miao, L. Wan, and Q. Ji, “Prediction-cgan: Human action prediction with conditional generative adversarial networks,” in *Proceedings of the 27th ACM International Conference on Multimedia (ACMMM)*, 2019, pp. 611–619.
- [51] Y. Kong, Z. Tao, and Y. Fu, “Adversarial action prediction networks,” *IEEE Transactions on Pattern Analysis and Machine Intelligence (TPAMI)*, vol. 42, no. 3, pp. 539–553, 2020.
- [52] X. Wu, J. Zhao, and R. Wang, “Anticipating future relations via graph growing for action prediction,” in *Proceedings of the AAAI Conference on Artificial Intelligence*, vol. 35, no. 4, 2021, pp. 2952–2960.
- [53] L. Van der Maaten and G. Hinton, “Visualizing data using t-sne.” *Journal of Machine Learning Research (JMLR)*, vol. 9, no. 11, 2008.